

Full Sheet Control Using Steerable Nips

Rene Sanchez, *Member, IEEE*, Roberto Horowitz, *Member, IEEE*, and Masayoshi Tomizuka, *Fellow, IEEE*

Abstract—This paper describes the mechatronics design, prototype testing and control of a steerable nips component for paper path mechanisms in high speed color printers and photocopiers. When placed upstream from the image transfer station along the paper path, this device precisely controls the longitudinal, lateral and skew directions of papers sheets, as they arrive to the image transfer station.

The paper also presents a complete kinematic and dynamic analysis of the paper sheet steering mechanism, which is validated by experimental results. It is shown that the dynamics of a sheet under the control of the steerable nips mechanism are nonlinear and subject to nonholonomic constraints. A feedback linearization control strategy that includes dynamic surface control is developed and implemented to control the sheet's position and angular orientation under the condition that the sheet's speed in the longitudinal direction remains positive at all times. Experimental results verify that the steerable nips mechanism under the proposed feedback linearization control strategy is able to meet or exceed all design performance requirements for deployment as a component of an actual printer paper path control mechanism.

Index Terms—paper sheet control, nonlinear control, state feedback linearization, nonholonomic.

I. INTRODUCTION

STATE of the art paper path control requires the sheets to be accurately positioned as they arrive to the image transfer station. This includes correction for longitudinal, lateral, and angular errors. To accomplish this task, current machines have a registration station at the end of the paper path and before the image transfer station, which must correct for lateral and skew errors and deliver the sheet to the image transfer station on time and with a constant longitudinal velocity. However, most state of the art registration devices can not correct for errors at high speeds, whereas others mark the paper since they rely on high contact point forces to move the sheet laterally. In this paper we present the mechatronics design, control and experimental verification of an innovative device, known as the Steerable Nips Mechanism [11] that permits a swifter correction of sheet lateral, longitudinal, and angular errors without marking the sheet. A prototype of this device was designed and built at the Department of Mechanical Engineering of University of California at Berkeley (UCB). The sheet actuation mechanism in this device consists of two rollers, which are free to rotate parallel and perpendicular to the sheet, and will henceforth be referred to as “steerable nips”. A freely rotating ball is spring-loaded against each of the steerable nips, providing a normal force that creates the friction force needed to propel the sheet through rolling, while minimizing the contact area between the steerable nip

and sheet; hence, decreasing the possibility of marking the sheet. By controlling the steering angle and spinning velocity of each of the two nips, it is possible to control the longitudinal position, lateral position and angular orientation of the sheet in a somewhat analogous manner to steering a two-wheel robot cf. [2], [29], [27], [28]. However, unlike the two-wheel robot steering control problem, the sheet control under the steerable nips mechanism proposed in this paper has an additional degree of freedom, since the paper sheet can buckle, whereas the pavement does not. As will be explained in subsequent sections, the buckling of the paper makes it possible to linearize the system dynamics through feedback, whereas feedback linearization cannot be achieved in the two-wheel robot steering problem. The control system for the steerable nips mechanism must be designed so the paper is neither folded nor stretched too severely to prevent the paper from tearing or having skid marks from the nips.

Prior recent work in the area of sheet control in a printer paper path has primarily focused on the design of control architectures and control algorithms for coordinating multiple actuated sections of the paper path, in order to correct for longitudinal inter-spacing errors among sheets, and synchronize the arrival of a sheet to the image transfer station with its corresponding image, with respect to both time and longitudinal velocity [26], [15], [14], [18], [4], [3], [16], [13], [5], [6], [1], [12]. However, none of these works address that issue of the simultaneous correction of paper sheet longitudinal, lateral and angular positioning errors, which is the focus of this paper. Prior works that address this issue are more scarce cf. [25] and is primarily in the form of patent disclosures. The description of the steerable nips mechanism in this paper, as well as its kinematic analysis, was first presented in [21]. However, because the fabrication of the steerable nips prototype was not completed, [21] only presented a simplified dynamic analysis of mechanism, which did not include actuators' dynamics, as well as a significantly simplified version of the feedback control scheme presented in this paper and some simulation results. [22] presents a hybrid automata-based control strategy for the model described in [21], which has four finite states among which the control system switches during the trajectory tracking process. It is shown in [22] that, by using a hybrid automata, it is possible to drive the paper from rest to any other position. [20] presented a more complete dynamic model of the steerable nips mechanism in this paper, which included actuators' dynamics, as well as experimental results, some of which are included in this paper. Recently, [7] presented a control strategy for an underactuated steerable nips mechanism for printer sheet registration devices that is similar to the device presented in this paper. However, since the mechanism in [7] has one less degree of freedom than the mechanism presented in this paper and no sheet buckling nor actuators'

This work was supported by the National Science Foundation under Grant CMS 0301719 and by financial support and collaboration from the Xerox Corporation

Manuscript received April 19, 2005; revised January 11, 2007.

dynamics is included in the control system design model, the control problem in [7] resembles more that of the steering a two-wheel robot, precluding the use of feedback linearization, and the resulting control strategy is significantly different from the one presented in this paper.

The objective of the steerable nips mechanism is to control the motion of a sheet of paper on an horizontal plane, from the time instant when the leading edge of the sheet enters in contact with the nips until the time instant when the trailing edge of the sheet losses contact with the nips, in order to reduce longitudinal, lateral and angular position tracking errors to acceptable levels before the sheet enters the image registration station. The control strategy presented in this paper uses linearization by state feedback [23] and a back-stepping technique similar to dynamic surface control [24], and considers a realistic steerable nip mechanism model that accounts for small amounts of sheet buckling and includes actuator dynamics. Simulation and experimental results are in close agreement and show that, by using the proposed control strategy, the steerable nips mechanism can correct for large initial sheet tracking errors, which exceed industry specifications, and attain sheet tracking errors when the sheet enters the registration station that are well below industry requirements without damaging the sheet.

Section II describes in detail the design process of some of the important components of the experimental setup. In order to derive a realistic model of the controlled plant, the dynamic models for each of the actuators were derived and validated with experimental data, this is the topic of section III. In Section IV we derive the kinematic model and in Section V we derive the overall dynamic model of the steerable nips mechanism. The control strategy developed to control paper position and orientation of a sheet are presented in Section VI. The model and experimental results are presented in Section VII. Finally, conclusions and some comments regarding the design, control strategies, and experimental results are stated in Section VIII.

II. EXPERIMENTAL SETUP

The fixture shown in Fig. 1 was designed to allow the steerable nips concept shown in Fig. 2, to be tested. This mechanism has two rotating steerable rollers, which propel while steering a sheet in the horizontal plane. The fixture also has an exit roller, which moves the sheets out of the fixture as trailing edge of the papers losses contact with the steerable nips, and a feeder unit that feeds the sheets into the fixture.

The steerable nips mechanism in Fig. 2 can correct for lateral errors in the sheet's initial position, in addition to longitudinal and angular errors, without laterally moving the rollers, as is the case of most current registration and deskewing systems. This is achieved by steering the paper sheet through the coordinated angular rotation and steering of the two rollers. The rollers are designed to have only a point of contact with the sheet, as shown in Fig.2. A ball is spring loaded on top of each rollers, providing a normal force that allows the rollers to drive the sheet. The combination of roller and ball is known as the nip. Properly controlled, the rollers can drive the sheet

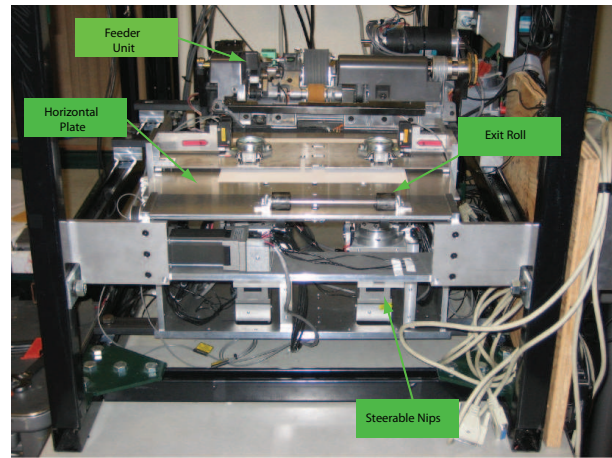


Fig. 1. Experimental Setup

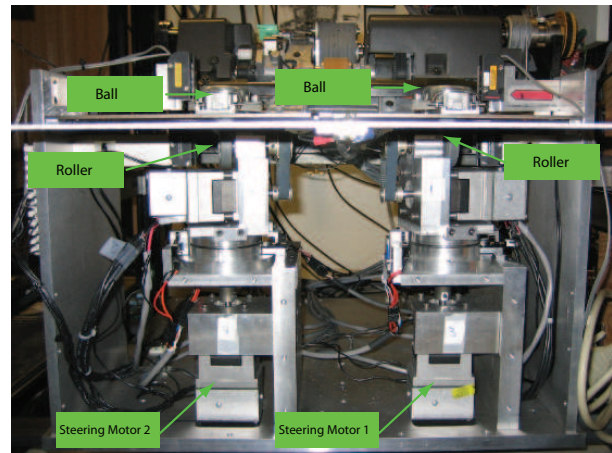


Fig. 2. Steerable Nips Mechanism

until its back edge exits the nips without inflicting any damage or visible skid marks on the sheet. Each roller is rotated by a servo motor, which will henceforth be referred to as the process motor, through a belt and pulleys as shown in Fig.2. The process motors were chosen to be light in weight and small in size, in order to minimize the steering inertia. The two rollers are separated by a distance of 200 mm. This spacing is compatible with standard sheet sizes. Each roller and its respective process motor are attached to a rotating table. The rotating table is steered by another servo motor, which will henceforth be referred to as the steering motor, as shown in Fig.3. This steering table is connected to the servo motor through a precision shaft coupling. This coupling allows the rotating table to be driven directly by the servo motor under small shaft misalignment. This is a desirable feature since an additional belt would have decreased the stiffness of the steering mechanism. The rotating table sits on a trust bearing that allows it to freely rotate while supporting its weight. There are also two ball bearings that prevent the rotating table from moving axially.

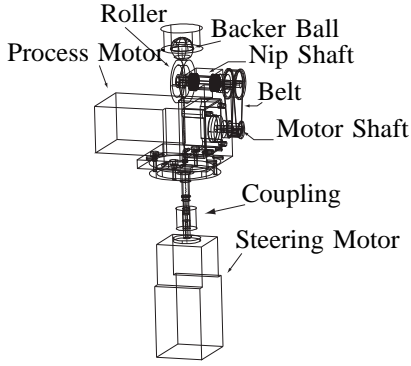


Fig. 3. Process Direction Actuator and Steering Motor Mechanism

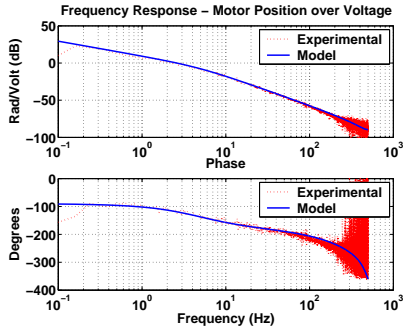


Fig. 4. Experimental and Modeled Frequency Response of Process Actuator

III. ACTUATOR DYNAMICS

There are four actuators in the steerable nips mechanism. Two of the actuators rotate each of the rollers and the other two steer them. In this section describe the dynamic model derivation, reduction and validation for each of the actuators of the experimental fixture.

A. Process Dynamics

The process actuators rotate the two rollers and each consists of a d.c. servo motor, which drives a roller through a timing belt, as shown in Fig. 3. A fifth order linear state space model of this actuator was derived, which accounted for the stiffness of the timing belt and inductance of the d.c. motor. The parameters of the model were determined through experimental frequency response tests and are listed in table I.

Figure 4 plots the experimental frequency response of the transfer function between the voltage input and the roller angular rotation output of the process actuator, as well as the corresponding frequency response of the derived fifth-order model. As shown in the figure, the model frequency response closely matches experimental data at frequencies below 100Hz.

The fifth-order process actuator model was reduced to a second order model, by neglecting the inductance of the d.c. motor and assuming that the timing belt connecting the two pulleys of the actuator is very stiff. The resulting transfer function between the input voltage and the roller angular rotation output is

Variable	Units	Description	Value
i	Amps	Current	
θ_m	rad	Motor Ang. Pos.	
θ_r	rad	Roller Ang. Pos.	
u	V	Motor Input	
K_t	$\frac{N-m}{Amp}$	Motor Torque Cons.	0.047
R	Ohms	Motor Res.	19.8
L	Hen	Motor Induc.	0.0071
J_m	$N-m^2$	Motor and Pulley Moments of Inertia	3.1e-6
J_r	$N-m^2$	Roller and Pulley Moments of Inertia	1.95e-006
J_b	$N-m^2$	Ball Moment of Inertia	2.3e-7
K	$\frac{N}{rad}$	Belt Spring Coef.	369.2
B	$\frac{N-sec}{rad}$	Belt Damping Coef.	1
Bf_m	$\frac{N-sec}{rad}$	Motor Visc. Fric.	6.5e-7
Bf_r	$\frac{N-sec}{rad}$	Roller Viscous Fric.	9.55e-6
Bf_b	$\frac{N-sec}{rad}$	Ball Visc. Fric.	3.50e-6
r_1	m	Motor Pulley Radius	0.0058
r_2	m	Roller Pulley Radius	0.012
r_3	m	Roller Radius	0.02
r_4	m	Ball Radius	0.011

TABLE I
PROCESS ACTUATOR VARIABLES AND EXPERIMENTALLY DETERMINED MODEL PARAMETERS

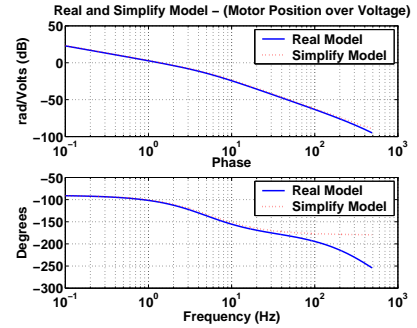


Fig. 5. Frequency Responses of the Process Motor High-order and Reduced-order Models

$$\ddot{\theta}_r + \alpha_p \dot{\theta}_r = \beta_p u \quad (1)$$

where

$$\alpha_p = \frac{Bf_r + \frac{r_3}{r_4} Bf_b + (Bf_m + \frac{K_t^2}{R}) \frac{r_2^2}{r_1^2}}{J_r + \frac{r_3^2}{r_4^2} J_b + \frac{r_2^2}{r_1^2} J_m} \quad \text{and} \quad \beta_p = \frac{\frac{r_1}{r_2} \frac{K_t}{R}}{J_r + \frac{r_3^2}{r_4^2} J_b + \frac{r_2^2}{r_1^2} J_m}$$

The frequency response of the simplified model, Eq. (1), can be seen in Fig. 5. It is shown that the magnitude of the second-order model closely matches the fifth-order model in the frequency range shown. As expected, the phase of the reduced-order model diverges from the fifth-order model at high frequencies.

B. Steering Dynamics

The steering actuator consists of a d.c. servo motor that rotates a table, as shown in Fig. 3. This table holds the process actuator and is connected to the motor through a coupling. A third order linear state space model of this actuator was derived, which accounted for inductance of the d.c. motor. The parameters of the model were determined through

Variable	Units	Description	Value
i	Amps	Current	
ϕ	rad	Steering Ang.	
u	V	Motor Input	
K_t	$\frac{N-m}{Amp}$	Motor Torque Cons.	0.05
R	Ohms	Motor Res.	6.78
L	Hen	Motor Ind.	0.0023
J_t	$N-m^2$	Total Moment of Inertia	6.24e-4
Bf_m	$\frac{N}{rad}$	Motor Visc. Fric.	1.4e-6

TABLE II

STEERING ACTUATOR VARIABLES AND EXPERIMENTALLY DETERMINED PARAMETER VALUES

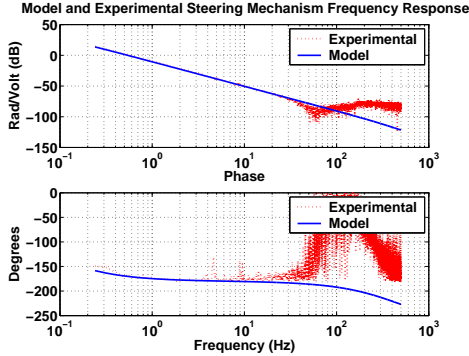


Fig. 6. Experimental and Modeled Steering Actuator Frequency Response

experimental frequency response tests and are listed in table II.

Figure 6 plots the experimental frequency response of the transfer function between the voltage input and the steering angular rotation, as well as the corresponding frequency response of the derived third-order model. As shown in the figure, the model frequency response closely matches experimental data at frequencies below 40 Hz.

The mismatch between the modeled and experimental results for frequencies higher than 40 Hz can be attributed to low signal to noise ratio. The system was excited with white noise and the excitation level did not produce a sufficiently large displacement at high frequency to overcome the encoder accuracy. The estimated values for the parameters of the steering actuators are also shown in Table II. As in the case of the process actuators, the dynamic model of the steering mechanism can be reduced by assuming that the inductance of the motor is negligible ($L \frac{di}{dt} \approx 0$). The resulting second order transfer function is given by

$$\ddot{\phi} + \alpha_s \dot{\phi} = \beta_s u \quad (2)$$

where

$$\alpha_s = \frac{(Bf + \frac{K_f^2}{R})}{J_t} \quad \text{and} \quad \beta_s = \frac{K_t}{J_t R}$$

The frequency response of the second-order and third-order models are shown in Fig. 7.

IV. KINEMATIC ANALYSIS

The steerable nips mechanism with a sheet is illustrated in Figs. (8) - (9). The steerable nips propel a sheet on a flat surface. Figure 8 represents the initial position of the sheet,

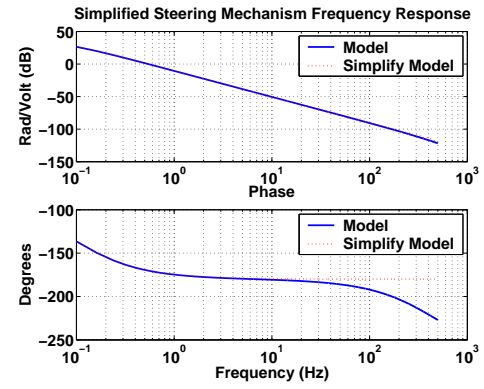


Fig. 7. High-order and Reduced-order Steering Actuator Frequency Response

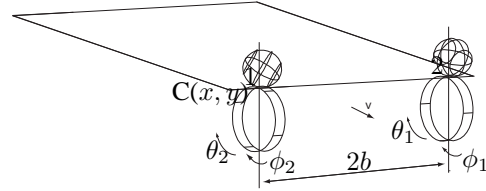


Fig. 8. Sheet Entering the Steerable Nips System

when it first makes contact with the nips. Figure 9 shows the sheet while it is being driven by the nips. The left corner of the sheet, point C , is used as a reference point for tracking. Note that even if the paper buckles, point C will remain on the flat surface since, buckling occurs only between points 1 and 2, where the sheet contacts the nips.

A. Kinematic Analysis Assumption

A key modeling assumption in the kinematic analysis that follows is that, even under buckling, the sheet remains transversally stiff and it rotates as a rigid body under the action of the steerable nips. This assumption is illustrated in Fig. 9, where any line perpendicular to the line that connects

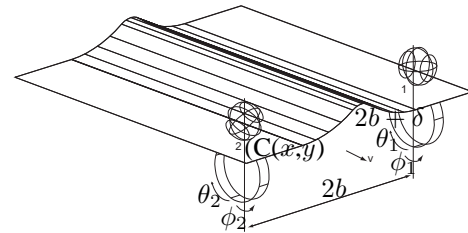


Fig. 9. Steerable Nips with Sheet Buckle

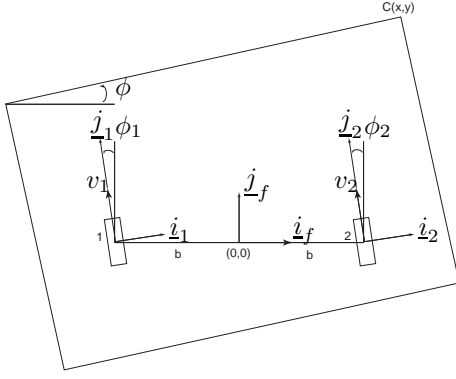


Fig. 10. System Coordinate

contact points 1 and 2, drawn along the buckled surface remains horizontal. Numerous experimental results confirmed the validity of this assumption to within possible measurement resolution.

B. Notation

Figure 10 shows a schematic representation of the kinematic variables for the steerable nips system. This system has two independent steering wheels, located at points 1 and 2. These steerable wheels are separated by a distance $2b$. Three coordinate frames are defined to describe the position and orientation of the paper sheet: a fixed global coordinate system denoted $(\underline{i}_f, \underline{j}_f, \underline{k}_f)$, and two local frames $(\underline{i}_1, \underline{j}_1, \underline{k}_1)$ and $(\underline{i}_2, \underline{j}_2, \underline{k}_2)$ attached to wheels 1 and 2 respectively. The generalized coordinates of the system are $(x, y, \phi, \delta, \theta_1, \theta_2, \phi_1, \phi_2)$. Generalized coordinates x and y will be used to respectively represent the lateral and longitudinal position of the leading right corner of the sheet (point C). Coordinate ϕ represents the angular (or skew) rotation of the sheet and $-\delta$ represents the amount of buckle experienced by the sheet, which we assume to only take place along the line that connects points 1 and 2. The angular position of wheel 1 in the directions parallel and perpendicular to the sheet are denoted as θ_1 and ϕ_1 respectively. Likewise, θ_2 and ϕ_2 describe the angular position of wheel 2 parallel and perpendicular to the sheet.

C. Velocity Analysis

The velocities of the paper at points 1 and 2 in global coordinates are:

$$\underline{v}_1 = (\dot{x} + \dot{\phi}y)\underline{i}_f + (\dot{y} - \dot{\phi}(x+b))\underline{j}_f - \dot{\delta}\underline{i}_f \quad (3)$$

$$\underline{v}_2 = (\dot{x} + \dot{\phi}y)\underline{i}_f + (\dot{y} + \dot{\phi}(-x+b))\underline{j}_f \quad (4)$$

where $\dot{\delta}$ is the rate of change of the sheet buckle (or stretch), which is assumed to only take place along the direction of the line that connects point 1 and 2 (along the \underline{i}_f unit vector). Notice that a negative δ implies that the sheet has buckled while a positive δ implies that the sheet has stretched. Invoking the non-slip condition, \underline{v}_1 and \underline{v}_2 can also be written in terms

of the angular speed of the wheels in the local coordinate frames:

$$\underline{v}_1 = -r_1\dot{\theta}_1\underline{j}_1 \quad (5)$$

$$\underline{v}_2 = -r_2\dot{\theta}_2\underline{j}_2 \quad (6)$$

where r_1 and r_2 are the radius of wheels 1 and 2 respectively.

Four constraint equations are obtained by writing Eqs. (5) and (6) in terms of the global coordinates and equating them to Eqs. (3) and (4).

$$\underline{v}_1 = -r_1\dot{\theta}_1[-\sin\phi_1\underline{i}_f + \cos\phi_1\underline{j}_f] \quad (7)$$

$$= (\dot{x} + \dot{\phi}y - \dot{\delta})\underline{i}_f + (\dot{y} - \dot{\phi}(x+b))\underline{j}_f$$

$$\underline{v}_2 = -r_2\dot{\theta}_2[-\sin\phi_2\underline{i}_f + \cos\phi_2\underline{j}_f] \quad (8)$$

$$= (\dot{x} + \dot{\phi}y)\underline{i}_f + (\dot{y} - \dot{\phi}(x-b))\underline{j}_f$$

These equations result in four nonholonomic constraints:

$$\dot{x} + \dot{\phi}y - \dot{\delta} = r_1 \sin\phi_1 \dot{\theta}_1 \quad (9)$$

$$\dot{y} - \dot{\phi}(x+b) = -r_1 \cos\phi_1 \dot{\theta}_1 \quad (10)$$

$$\dot{x} + \dot{\phi}y = r_2 \sin\phi_2 \dot{\theta}_2 \quad (11)$$

$$\dot{y} - \dot{\phi}(x-b) = -r_2 \cos\phi_2 \dot{\theta}_2 \quad (12)$$

Defining the generalized coordinate $p = [x \ y \ \phi \ \delta \ \theta_1 \ \theta_2 \ \phi_1 \ \phi_2]^T$, the constraints can be written in Pfaffian form [17] as:

$$A(p)\dot{p} = 0 \quad (13)$$

where $A(p)$ is the 4×8 matrix defined below.

$$A(p) = \begin{bmatrix} 1 & 0 & y & -1 & -r_1 \sin\phi_1 & 0 & 0 & 0 \\ 0 & 1 & -(x+b) & 0 & r_1 \cos\phi_1 & 0 & 0 & 0 \\ 1 & 0 & y & 0 & 0 & -r_2 \sin\phi_2 & 0 & 0 \\ 0 & 1 & -(x-b) & 0 & 0 & r_2 \cos\phi_2 & 0 & 0 \end{bmatrix}$$

D. Kinematic Equations

The kinematic model represents the relation between the moving parts of the system, when they comply with the nonholonomic constraints describe earlier. As detailed in [17] this is given by a basis of the right null space of the constraints, $a_i(p)$, which will be denoted by $g_j(p) \in \mathbb{R}^n$, $j = 1, \dots, n - k = m$. By construction, this basis satisfies:

$$a_i(p)g_j(p) = 0 \quad i = 1, \dots, k \quad j = 1, \dots, n - k \quad p \in \mathbb{R}^n$$

and all allowable trajectories of the system can thus be written as the possible solutions of the system

$$\dot{p} = g_1(p)u_1 + \dots + g_m(p)u_m. \quad (14)$$

That is, $p(t)$ is a feasible trajectory of the system if and only if $p(t)$ satisfies Eq. (14) for a choice of control $u(t) \in \mathbb{R}^m$.

For our system this basis are easily obtained and the solution can be written as follows

$$\dot{x} = -\frac{yr_1}{2b} \cos \phi_1 \dot{\theta}_1 + \left(\frac{yr_2}{2b} \cos \phi_2 + r_2 \sin \phi_2 \right) \dot{\theta}_2 \quad (15)$$

$$\dot{y} = \left(\frac{(x+b)r_1}{2b} \cos \phi_1 - r_1 \cos \phi_1 \right) \dot{\theta}_1 - \frac{(x+b)r_2}{2b} \cos \phi_2 \dot{\theta}_2 \quad (16)$$

$$\dot{\phi} = \frac{1}{2b} (r_1 \cos \phi_1 \dot{\theta}_1 - r_2 \cos \phi_2 \dot{\theta}_2) \quad (17)$$

$$\dot{\delta} = r_2 \sin \phi_2 \dot{\theta}_2 - r_1 \sin \phi_1 \dot{\theta}_1 \quad (18)$$

which constitute the kinematic model of our system. Notice that Eqs. (15)-(18) can be succinctly written as follows

$$\dot{\underline{y}} = G(\underline{y}, \eta) \eta \quad (19)$$

where the output

$$\underline{y} = [x \quad y \quad \phi \quad \delta]^T$$

are the generalized coordinate vector of the paper sheet, with elements given respectively by the lateral and longitudinal coordinates x and y for the sheet's leading edge right corner C (see Fig. 10), the sheet angular rotation ϕ and the buckle δ , and

$$\eta = [\dot{\theta}_1 \quad \dot{\theta}_2 \quad \phi_1 \quad \phi_2]^T$$

is the input vector formed by the the nips' rotor angular speeds and steering angles.

E. Sheet Motion Sensing and Kinematic Model Experimental Validation

An array of optical sensors, located along the longitudinal direction in the midpoint between the two rollers, as shown in Fig. 11, were used to detect the leading edge of the sheet. Three laser sensors, two of which are located on the right side of the sheet at locations $(\bar{x}, -d_s)$ and $(\bar{x}, 0)$ respectively, and one is located on the left size of the sheet, at location $(-\bar{x}, 0)$, as shown in Fig. 11, were used to measure the lateral deviation of the sheet edge relative to the sensor location (e.g. s_1 and s_2 are zero if the right-hand sheet edge is on top of both sensors). The amount of buckle $-\delta$ was determined from the readings

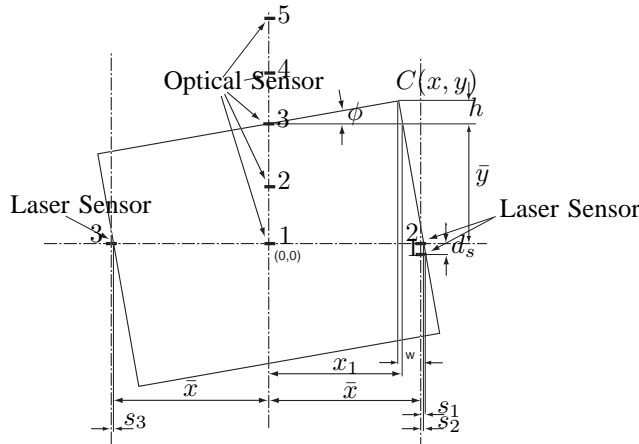


Fig. 11. Sheet Position from Optical and Laser Sensors

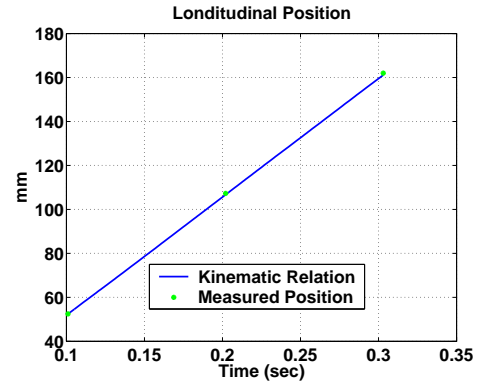


Fig. 12. Predicted and Measured Sheet Longitudinal Position

s_2 and s_3 of the two laser sensors located on opposite sides of the sheet, while the angular position of the sheet, ϕ , was determined from readings s_1 and s_2 of the two laser sensors on the right side of the sheet. They are respectively given by

$$\delta = s_2 - s_3 \quad \phi = \tan^{-1} \left(\frac{s_1 - s_2}{d_s} \right) \quad (20)$$

where d_s is the longitudinal distance between the two laser sensors 1 and 2, as shown in Fig. 11.

The position of point $C(x, y)$ on the right side of the leading edge of the sheet was determined every time the leading edge of the sheet went over one of the optical sensors. The longitudinal position of each sensor that is being crossed is denoted by \bar{y} and the distance from the center (zero value), then the coordinates y and x of the point $C(x, y)$ are respectively given by

$$\begin{aligned} y &= \bar{y} + (\bar{x} - \bar{y} \tan \phi + s_2) \sin \phi \cos \phi \\ x &= \bar{x} - y \tan \phi, \end{aligned} \quad (21)$$

where $2\bar{x}$ is the lateral distance between laser sensors 2 and 3 (see Fig.11). The kinematic state-model equations given by Eqs. (19) were validated using the following procedure: First, a sheet of paper was fed into and controlled by the steerable nips mechanism until it exited, while all sensor data was collected and stored. Secondly, the initial generalized coordinate vector of the paper sheet $\underline{y}(0)$ was set to the values either directly measured or computed from Eqs. (20)-(21) at the instant when the leading edge of the sheet went over the first optical longitudinal sensor. Subsequently, Eqs. (19) were numerically integrated using as inputs the measured roller angular speed and steering angle of each nip. Finally the numerically integrated sheet longitudinal, lateral and angular positions $(y(t), x(t), \phi(t))$ were plotted along with actual values computed from Eqs. (20)-(21) at the instances when the leading edge of the sheet went over one of the optical longitudinal sensors. Typical results are shown in Figs. 12-14.

Notice that there is a close match between the measured and predicted data in spite of the fact that the edges of paper sheets are not perfectly straight, and the data was contaminated by sensor and quantization noise. The angular velocities and steering angles used for the experimental validation of the kinematic equations were chosen in order not to induce

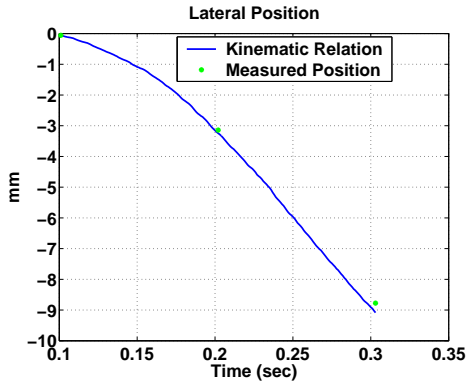


Fig. 13. Predicted and Measured Lateral Sheet Position

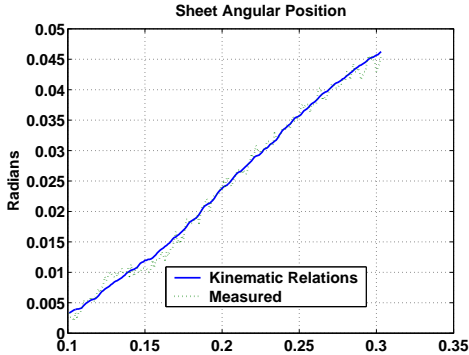


Fig. 14. Predicted and Measured Sheet Angular Position

appreciable buckle. Whatever buckle values were obtained from measurements and Eq. (20) was within the range of error attributed to the fact that the sheets are not all exactly the same length and their edges are not parallel to each other.

V. DYNAMIC MODEL

A. Dynamic Analysis Assumptions

The key modeling assumption used in the dynamic analysis that follows is that the mass of the sheet is small and, therefore, it can be neglected. As a consequence, the overall model of the steerable mechanism consists of the dynamics of the actuators and the kinematic relation between the roller and the sheet. We also assume that a minute stretching of the sheet will not introduce dynamic coupling between the process and steering motors. These assumptions were also verified with numerous experimental results.

B. Dynamic System with Reduced-order Servo Dynamics

In this Section we derived a model based on the actuator dynamics presented in Section (III-A) and (III-B). These models have the following simplified form:

$$\ddot{\theta}_i + \alpha_i \dot{\theta}_i = \beta_i u_i \quad (22)$$

where α_i and β_i ($i = 1, 2, 3, 4$) represent physical characteristics of each actuator defined in Eq. (1) and (2). Inputs u_1 , u_2 , u_3 and u_4 are motor voltages to each of the servo motors.

Making use of the kinematic equations derived in section IV-D, Eq. (19) and its time derivative can be expressed as follows:

$$\ddot{\underline{y}} = M(\underline{x}) + N(\underline{x}) \begin{bmatrix} \ddot{\theta}_1 \\ \ddot{\theta}_2 \\ \dot{\phi}_1 \\ \dot{\phi}_2 \end{bmatrix} \quad (23)$$

$$\underline{y} = [x \ y \ \phi \ \delta]^T$$

$$\underline{x} = [x \ y \ \phi \ \delta \ \phi_1 \ \phi_2 \ \dot{\theta}_1 \ \dot{\theta}_2 \ \dot{\phi}_1 \ \dot{\phi}_2]^T$$

where \underline{y} is the output vector, the vector $M(\underline{x}) \in \mathcal{R}^3$ is given by

$$M(\underline{x}) = \begin{bmatrix} -\dot{\phi}\dot{y} \\ \dot{\phi}\dot{x} \\ 0 \\ 0 \end{bmatrix} \quad (24)$$

where the symbols \dot{x} , \dot{y} , $\dot{\phi}$ and $\dot{\delta}$ should be respectively replaced by the right hand side of Eqs. (15)-(18), and the elements of the matrix $N(\underline{x}) \in \mathcal{R}^{3 \times 3}$ are

$$\begin{aligned} n_{11} &= -\frac{yr_1}{2b} \cos \phi_1 & n_{12} &= \frac{yr_2}{2b} \cos \phi_2 + r_2 \sin \phi_2 \\ n_{13} &= \frac{yr_1}{2b} \sin \phi_1 \dot{\theta}_1 & n_{14} &= -\frac{yr_2}{2b} \sin \phi_2 \dot{\theta}_2 + r_2 \cos \phi_2 \dot{\theta}_2 \\ n_{21} &= -r_1 \cos \phi_1 + \frac{(x+b)r_1}{2b} \cos \phi_1 & n_{22} &= -\frac{(x+b)r_2}{2b} \cos \phi_2 \\ n_{23} &= r_1 \sin \phi_1 \dot{\theta}_1 - \frac{(x+b)r_1}{2b} \sin \phi_1 \dot{\theta}_1 & n_{24} &= \frac{(x+b)r_2}{2b} \sin \phi_2 \dot{\theta}_2 \\ n_{31} &= \frac{r_1}{2b} \cos \phi_1 & n_{32} &= -\frac{r_2}{2b} \cos \phi_2 \\ n_{33} &= -\frac{r_1}{2b} \sin \phi_1 \dot{\theta}_1 & n_{34} &= \frac{r_2}{2b} \sin \phi_2 \dot{\theta}_2 \\ n_{41} &= -r_1 \sin \phi_1 & n_{42} &= r_2 \sin \phi_2 \\ n_{43} &= -r_1 \cos \phi_1 \dot{\theta}_1 & n_{44} &= r_2 \cos \phi_2 \dot{\theta}_2 \end{aligned}$$

It should be emphasized that a necessary and sufficient condition for the matrix $N(\underline{x})$ to remain nonsingular is that the longitudinal speed, \dot{y} should remain positive.

The overall dynamic system model is given by

$$\ddot{\underline{y}} = M(\underline{x}) + N(\underline{x}) \begin{bmatrix} \ddot{\theta}_1 \\ \ddot{\theta}_2 \\ \dot{\phi}_1 \\ \dot{\phi}_2 \end{bmatrix}, \quad \begin{cases} \ddot{\theta}_1 + \alpha_1 \dot{\theta}_1 = \beta_1 u_1 \\ \ddot{\theta}_2 + \alpha_2 \dot{\theta}_2 = \beta_2 u_2 \\ \dot{\phi}_1 + \alpha_3 \dot{\phi}_1 = \beta_3 u_3 \\ \dot{\phi}_2 + \alpha_4 \dot{\phi}_2 = \beta_4 u_4 \end{cases} \quad (25)$$

VI. NONLINEAR CONTROL STRATEGY

The control objective in this paper is to control a sheet on the horizontal plane from an initial state with nonzero longitudinal velocity to a final state also with nonzero longitudinal velocity. The control strategy presented in this section assumes a realistic second order model for all actuators, as derived and validated in Section V-B. The control strategy developed for this system is also dynamic and uses concepts of linearization by state feedback [23] and a back-stepping technique similar to dynamic surface control [24]. The desired sheet trajectories lateral and longitudinal coordinates x and y for the sheet's leading edge right corner C , the sheet angular rotation ϕ and the buckle δ are given by

$$\begin{aligned} x_d(t) &= \dot{x}_d(t) = \ddot{x}_d(t) = 0 \\ y_d(t) &= \alpha t, \quad \dot{y}_d(t) = \alpha, \quad \ddot{y}_d(t) = 0 \\ \phi_d(t) &= \dot{\phi}_d(t) = \ddot{\phi}_d(t) = 0 \\ \delta_d(t) &= -c_1, \quad \dot{\delta}_d(t) = \ddot{\delta}_d(t) = 0 \end{aligned} \quad (26)$$

for $t = [0, T]$, where α and T are respectively the desired longitudinal velocity of the sheet and time at which the sheet must leave the steerable nips mechanism. The amount of buckle is c_1 . The block diagram of the proposed control strategy is shown in Fig. 15. The control law is given by Eq. (27) and Eq. (28):

$$\begin{bmatrix} \ddot{\theta}_{1d} \\ \ddot{\theta}_{2d} \\ \dot{\phi}_{1d} \\ \dot{\phi}_{2d} \end{bmatrix} = N(\underline{x})^{-1} \left(\begin{bmatrix} \ddot{x}_d + (K_1 + \lambda_1)\dot{\tilde{x}} + \lambda_1 K_1 \tilde{x} \\ \ddot{y}_d + (K_2 + \lambda_2)\dot{\tilde{y}} + \lambda_2 K_2 \tilde{y} \\ \ddot{\phi}_d + (K_3 + \lambda_3)\dot{\tilde{\phi}} + \lambda_3 K_3 \tilde{\phi} \\ \ddot{\delta}_d + (K_4 + \lambda_4)\dot{\tilde{\delta}} + \lambda_4 K_4 \tilde{\delta} \end{bmatrix} - M(\underline{x}) \right) \quad (27)$$

$$\begin{aligned} C_1(s) &= \frac{k_{p1}(s+\gamma_1)(s+\gamma_2)}{s^2} & C_2(s) &= \frac{k_{p2}(s+\gamma_3)(s+\gamma_4)}{s^2} \\ C_3(s) &= \frac{k_{s1}(s+\eta_1)}{s(s+\eta_2)} & C_4(s) &= \frac{k_{s2}(s+\eta_3)}{s(s+\eta_4)} \end{aligned} \quad (28)$$

Equation (27), which is schematically depicted in Fig. 15 by

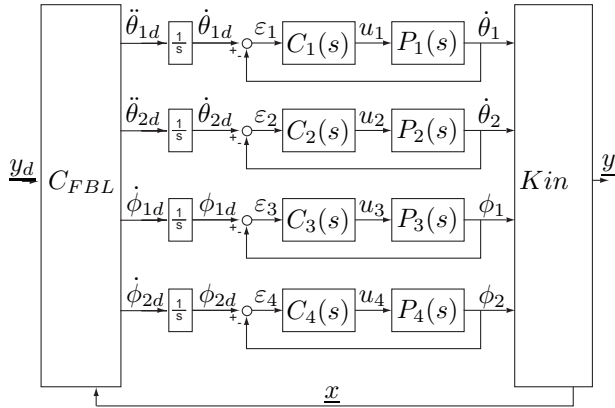


Fig. 15. Control System Block Diagram

the block C_{FBL} , linearizes through feedback the kinematics and generates the desired angular accelerations and desired steering velocities for each of the rollers. These desired values are then integrated to obtain reference trajectories, which are tracked by local inner linear controllers given by Eqs. (28) and represented by the blocks $C_i(s)$, $i = 1, 2, 3, 4$ in Fig. 15, where η_i and γ_i ($i=1,2,3,4$) are positive coefficients. The actuators' process dynamics are represented by the blocks $P_1(s)$, $i = 1, 2$ in Fig. 15 while the steering dynamics are represented by the blocks $P_i(s)$, $i = 3, 4$.

[19], [10], [9] provide a formal convergence analysis of this control strategy. Moreover, they also provide a systematic methodology to tune the control system so that, given a specified maximum nominal longitudinal speed α and a minimum travel time $T = \frac{\alpha}{L}$, where L is the length of the sheet, control gains can be determined so that the magnitude of tracking errors are guaranteed to be attenuated, from specified maximum initial values, to final values that are within specified allowable values.

In the control strategy in Eqs. (27) and (28) feedback linearization is used only to linearize the kinematics of the system, while internal loops are used to locally control the actuators positions and velocities. Through extensive simulation and experimental results, such as those presented in section VII, we have found that this control strategy performs robustly to parameter and dynamic uncertainty in the actuators. This robustness can be attributed to the fact the feedback

linearization portion of the controller does not depend on the actuator dynamics. In contrast, we have found [8] that control strategies that are based on direct output feedback linearization plus dynamic extension [23] of the overall plant given Eq. (25) do not perform well, under identical conditions, due to parameter and dynamic uncertainty in the actuators. [8] also presents a comprehensive robustness analysis which shows that the control strategy based on kinematic feedback linearization with actuator internal loops is significantly more robust to parameter and dynamic uncertainty in the actuators than the control strategy that is based on the direct output feedback linearization plus dynamic extension of the overall dynamics.

VII. SIMULATION AND EXPERIMENTAL RESULTS

Simulated and experimental results were obtained for a sheet with initial conditions as shown in Table IV. The values for the above control parameters are shown in Table III. Each of the control gains is the combination of all system gains such as gains of the amplifier, conversion factor from radians to encoder pulses, etc. The sheet was steered from this initial condition to a desired longitudinal, lateral, and angular position. In addition, the sheet was kept with a small amount of buckle to avoid stretching the sheet. Figure 16(a) shows the sheet longitudinal and lateral errors, and Fig. 16(b) shows the angular position and amount of paper buckle. The errors were reduced in the time allowed, less than 0.382 seconds. This time is dependent in the sheet velocity, the amount of skew error, the gap between lateral sensors and the sizes of a sheet. For example, for an A4 sheet ($194.6mm \times 279.4mm$) traveling at the velocity of $0.5m/sec$ with a maximum angular error of $0.025 radians$ and a sensor gap of $21.3 mm$ results in a allowable time of $0.382 seconds$ for correction for all errors. The final errors are within the requirements: less than $\pm 1.3mm$ in the lateral direction, $\pm 1.6mm$ in the process direction and $\pm 3.5mrad$ of angular error. Experimental and simulated results of sheet errors in Fig. 16(a) and 16(b) show some discrepancies. These discrepancies can be attributed to sensor noise and slip between the ball and the sheet. The rollers' angular velocities and steering angular positions are shown in Fig. 17(a) and 17(b). As it was expected the initial and final angular velocities are equivalent to the sheet's nominal longitudinal velocity once the errors have been corrected. The steering angular position of each roller is close to zero once the sheet's errors have been corrected.

Current sensing equipments limit the control precision at high speeds. Laser sensors noise level increases at high speeds decreasing the precision of sensors.

VIII. CONCLUSION

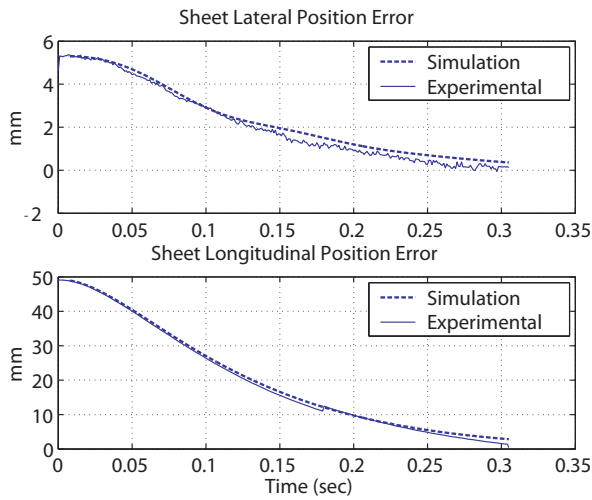
This paper presented an innovative mechanism to improve paper handling performance in a printer paper handling system, when it is placed before the image registration station. This mechanism uses steerable nips to control the motion of a sheet of paper on an horizontal plane, from the time instant when the leading edge of the sheet enters in contact with the nips until the time instant when the trailing edge of the sheet losses contact with the nips and enters the registration station,

Variable	Value
k_{p1}	0.5
k_{p2}	0.5
γ_1	20.7
γ_2	29.0
γ_3	20.7
γ_4	29.0
k_{s1}	1200
k_{s2}	1200
η_1	7.6
η_2	14.6
η_3	7.6
η_4	14.6

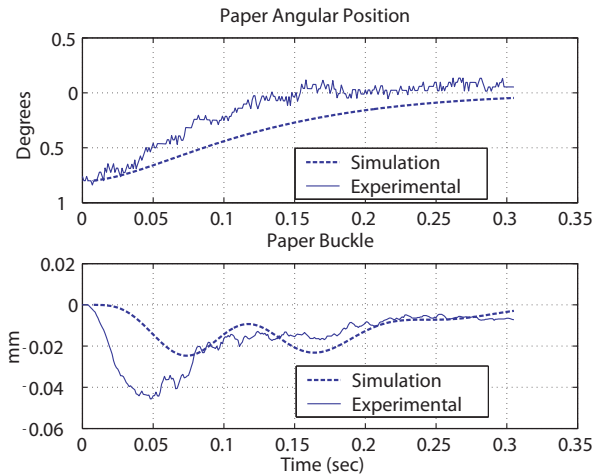
TABLE III
CONTROL VARIABLES

Variable Name	Value	Units
Sheet Lateral Error	5.2	millimeters
Sheet Longitudinal Error	-50	millimeters
Sheet Angle Position	0.7	degrees
Buckle	0	millimeters
Forward Velocity	0.5	meters/second
Available Control Time	0.35	seconds

TABLE IV
INITIAL EXPERIMENTAL AND SIMULATED SHEET ERRORS

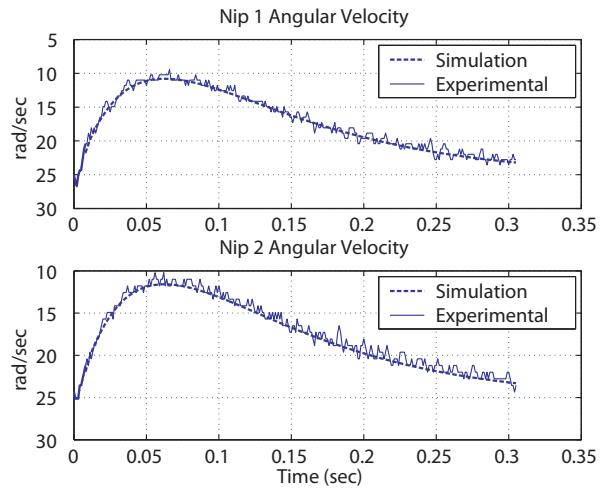


(a)

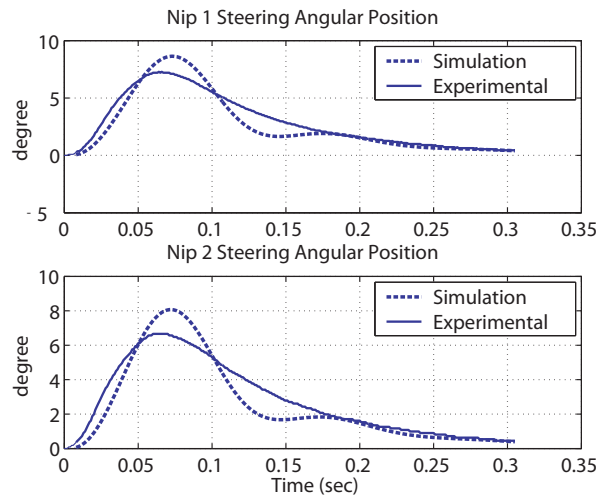


(b)

Fig. 16. (a) Sheet Lateral and Longitudinal Errors; (b) Sheet Angular Position and Sheet Buckle



(a)



(b)

Fig. 17. (a) Roller Angular Velocity; (b) Roller Steering Angle

in order to reduce longitudinal, lateral and angular position tracking errors to acceptable levels.

A prototype if this device was constructed and tested. Kinematic and dynamic models of the steerable nips mechanism were derived under the assumptions that the mass of the sheet can be neglected and that the paper sheet remains sufficiently stiff under minute levels of buckling to sustain rigid body rotation, and were validated with experimental data. A control strategy was presented in this paper comprising of a nonlinear outer feedback linearization loop, and inner dynamic surface control loops around each of the actuators. The outer loop linearizes the paper sheet kinematics under the steerable nips mechanism action, and generates a desired rotating speeds and steering angles for each two steerable nips. These reference trajectories are tracked by the four inner dynamic surface control feedback loops. Simulation and experimental results are in close agreement and show that, by using the proposed control strategy, the steerable nips mechanism can correct for large initial sheet tracking errors, which exceed industry specifications, and attain sheet tracking errors that are below

industry requirements when the sheet enters the registration station, without damaging or marking the sheet. Small discrepancies between the experimental and simulation results were attributed to sensor noise, irregularities in the edge of the paper and slight model parameter mismatches, particularly among the damping ratios of the actuators dynamics.



Dr. Sanchez is a member of IEEE and ASME.

Rene Sanchez Rene Sanchez was born in Gualaceo, Ecuador in 1970. He received both his B.S. and M.S. degrees in mechanical engineering from Rensselaer Polytechnic Institute in 1993 and 1995 respectively. He received his Ph.D. degree from the University of California at Berkeley in 2006. His industry experience includes Xerox Research Center from 1995 to 2000 and Nikon Research Corporation of America from 2006 to present. His research interests are nonlinear, learning, motion, and adaptive control related to robotics, precision movement, and manufacturing.



computer disk file systems, robotics, mechatronics and Intelligent Vehicle and Highway Systems (IVHS). Dr. Horowitz is a member of IEEE and ASME.

Roberto Horowitz Roberto Horowitz was born in Caracas, Venezuela in 1955. He received a B.S. degree with highest honors in 1978 and a Ph.D. degree in 1983 in mechanical engineering from the University of California at Berkeley. In 1982 he joined the Department of Mechanical Engineering at the University of California at Berkeley, where he is currently a Professor. Dr. Horowitz teaches and conducts research in the areas of adaptive, learning, nonlinear and optimal control, with applications to Micro-Electromechanical Systems (MEMS), com-



puter disk file systems, robotics, mechatronics and Intelligent Vehicle and Highway Systems (IVHS). Dr. Horowitz is a member of IEEE and ASME.

Masayoshi Tomizuka (M'86-SM'95-F'97) was born in Tokyo, Japan in 1946. He received the B.S. and M.S. degrees in mechanical engineering from Keio University, Tokyo, Japan and the Ph. D. degree in Mechanical Engineering from the Massachusetts Institute of Technology in February 1974. Currently, he holds the Cheryl and John Neerhout, Jr., Distinguished Professorship Chair at the University of California at Berkeley, where he has been since 1974. He teaches courses in dynamic systems and controls. His current research interests are optimal and adaptive control, digital control, signal processing, motion control, and control problems related to robotics, machining, manufacturing, information storage devices and vehicles. He has served as a consultant to various organizations, including General Electric, General Motors and United Technologies. Dr. Tomizuka was Technical Editor of the ASME Journal of Dynamic Systems, Measurement and Control, J-DSMC from 1988 to 1993, and Editor-in-Chief of the IEEE/ASME Transactions on Mechatronics from 1997 to 1999. He served as President of the American Automatic Control Council (AACC) from 1998 to 1999. He served as Program Director of the Dynamic Systems and Control Program in the Civil and Mechanical Systems Division of the National Science Foundation from 2002 to 2004. He is a Fellow of the American Society of Mechanical Engineers (ASME) and the Society of Manufacturing Engineers. He received, the Charles Russ Richards Memorial Award from ASME in 1997, the Rufus Oldenburger Medal from ASME in 2002 and John R. Raggazini Award from AACC in 2006.

REFERENCES

- [1] Bukkems B., van de Molengraft R., Heemels M., van de Wouw N., and Steinbuch M. A piecewise linear approach towards sheet control in a printer paper path. In *American Control Conference*, 2006.
- [2] G. Campion, d'Andrea Novel, and G. Bastin. Controllability and state feedback stabilisability of nonholonomic mechanical systems. In *Advanced robot control : proceedings of the International Workshop on Nonlinear and Adaptive Control: Issues in Robotics*, pages 106–124, Grenoble, November 1990.
- [3] Carlo Cloet, Martin Kruciński, Roberto Horowitz, and Masayoshi Tomizuka. A hybrid control scheme for a copier paperpath. In *1999 American Control Conference, San Diego*, pages TM05–4, June, 1999.
- [4] Carlo Cloet, Martin Kruciński, Roberto Horowitz, and Masayoshi Tomizuka. Intersheet spacing control and controllability of a copier paperpath. In *1998 IEEE Conference on Control Applications, Trieste, Italy*, pages TA–06, September, 1998.
- [5] Carlo Cloet, Masayoshi Tomizuka, and Roberto Horowitz. Design requirements and reference trajectory generation for a copier paperpath. In *Conference on Advanced Intelligent Mechatronics, Como, Italy, July, 2001*.
- [6] C. Clote. *A mechatronics approach to copier paperpath design*. PhD thesis, University of California, Berkeley, 2001.
- [7] Jack G. Elliot and Roger F. Gans. Closed-loop control of an under-actuated sheet registration device using feedback linearization and gain scheduling. *To appear in the IEEE Transaction on Control Systems Technology*, 2008.
- [8] Edgar Ergueta, , Robert Seifried, and Roberto Horowitz. A robust approach to dynamic feedback linearization for steerable nips mechanism. In *To be presented at the the 2008 ASME Dynamic Systems and Control Conference*, Ann Arbor, MI, October 2008.
- [9] Edgar Ergueta, Rene Sanchez, Roberto Horowitz, and Masayoshi Tomizuka. Convergence analysis of a steerable nips mechanism for full sheet control in printing devices. Submitted to the ASME Journal of Dynamic Systems Measurement and Control, 2007.
- [10] Edgar Ergueta, Rene Sanchez, Roberto Horowitz, and Masayoshi Tomizuka. Full sheet control through the use of steer-able nips. In *Proceeding of the 2007 ASME IMECE Paper Number IMECE2007-41279*, Seattle, WA, November 2007.
- [11] NY) Hwang, Shyshung S. (Penfield. Sheet registration and deskewing system with independent drives and steering. United States Patent Number 6634521, October 2003.
- [12] de Best JJTH, Bukkems BHM, van de Molengraft MJG, Heemels WPMH, and Steinbuch M. Robust control of piecewise linear systems: A case study in sheet flow control. *Control Engineering Practice*, 16(8):991–1003, August 2008.
- [13] Martin Krucinski. *Feedback Control of Photocopying Machinery*. PhD thesis, University of California Berkeley, 2000.
- [14] Martin Krucinski, Carlo Cloet, Roberto Horowitz, and Masayoshi Tomizuka. Asynchronous observer for a copier paperpath. In *37th IEEE Conference on Decision and Control*, volume 3, pages 2611–2612, December 1998.
- [15] Martin Kruciński, Carlo Cloet, Roberto Horowitz, and Masayoshi Tomizuka. Interobject spacing control and controllability of a manufacturing transportation system. In *1998 American Control Conference*, volume 2, pages 1259–1265, June 1998. Session WA03-4.
- [16] Martin Kruciński, Carlo Cloet, Roberto Horowitz, and Masayoshi Tomizuka. A mechatronics approach to copier paperpath control. In *1st IFAC Conference on Mechatronic Systems, Darmstadt, Germany*, September, 2000.
- [17] Richard M. Murray, Zexiang Li, and Shankar S. Sastry. *A Mathematical Introduction to Robotic Manipulation*. CRC Press, 1993.
- [18] Sudhendu Rai and Warren Jackson. A hybrid hierarchical control architecture for paper transport systems. In *37th IEEE Conference on Decision and Control, Tampa, Florida*, pages FP01–6, December, 1998.
- [19] R. Sanchez. *Nonlinear Control Strategies for a Steerable Nips Mechanism*. PhD thesis, University of California, Berkeley, 2006.
- [20] Rene Sanchez, Edgar Ergueta, Benjamin Fine, Roberto Horowitz, Masayoshi Tomizuka, and Martin Krucinski. A mechatronic approach to full sheet control using steer-able nips. In *Proceedings of the 4th IFAC-Symposium on Mechatronic Systems, Heidelberg, Germany, September 2006*.
- [21] Rene Sanchez, Roberto Horowitz, and Masayoshi Tomizuka. Paper sheet control using steerable nips. In *2004 American Control Conference Proceedings*, pages 482–487, Boston, Massachusetts, June 30–July 2 2004.

- [22] Rene Sanchez, Roberto Horowitz, Masayoshi Tomizuka, and Slobodan N. Simić. Full paper sheet control using hybrid automata. In *Hybrid Systems : Computation and Control 2004 Proceedings*, pages 523–538, Philadelphia, Pennsylvania, March 2004.
- [23] S. S. Sastry. *Nonlinear Systems : Analysis, Stability, and Control*. Springer, 1999.
- [24] D. Swaroop, J. C. Gerdes, P. P. Yip, and J. K. Hedrick. Dynamic surface control of nonlinear systems. In *Proceedings of the American Control Conference*, volume 5, pages 3028 –3034, Albuquerque, New Mexico, June 1997.
- [25] Naoya Tanaka, Hiroshi Fukumoto, Kazuaki Arimoto, and Yoshitaka Iwashita. Skew correction mechanism for thermal transfer type color printers. In *International Conference on Micromechatronics for Information and Precision Equipment, Tokyo*, pages 635–638, July 1997.
- [26] Per Tunestål and Martin Kruciński. Hybrid control of a manufacturing transport system. In *1997 IEEE Conference on Decision and Control, San Diego*, pages Session ID WA03–4, December, 1997.
- [27] D. Wang and G. Xu. Full-state tracking and internal dynamics of nonholonomic wheeled mobile robots. *TRANSACTIONS ON MECHATRONICS, IEEE/ASME*, pages 203–14, June 2003.
- [28] Y. Xu and S. Kwok-Wai Au. Stabilization and path following of a single wheel robot. *TRANSACTIONS ON MECHATRONICS, IEEE/ASME*, pages 407–19, June 2004.
- [29] Xiaoping Yun and N. Sarkar. Dynamic feedback control of vehicles with two steerable wheels. In *1996 IEEE International Conference on Robotics and Automation*, pages 3105–3110, 1996.